tvst

Cornea & External Disease

Therapeutic Ultrasound for Topical Corneal Delivery of Macromolecules

Hanaa H. Almogbil[1], Felipe Montecinos-Franjola[2], Camille Daszynski[1], William J. Conlon[2], Justin S. Hachey[2], Giavanna Corazza[1], Erik A. Rodriguez[2], and Vesna Zderic[1]

[1] Department of Biomedical Engineering, The George Washington University, Washington, DC, USA
[2] Department of Chemistry, The George Washington University, Washington, DC, USA

Correspondence: Vesna Zderic, Department of Biomedical Engineering, School of Engineering and Applied Science, The George Washington University, 800 22nd Street NW, Room 6670, Washington, DC 20052, USA.
e-mail: zderic@gwu.edu

Received: April 26, 2022
Accepted: July 23, 2022
Published: August 23, 2022

Keywords: therapeutic ultrasound; cornea; drug delivery; macromolecules; small ultra-red fluorescent protein (smURFP); fluorescence imaging

Citation: Almogbil HH, Montecinos-Franjola F, Daszynski C, Conlon WJ, Hachey JS, Corazza G, Rodriguez EA, Zderic V. Therapeutic ultrasound for topical corneal delivery of macromolecules. Transl Vis Sci Technol. 2022;11(8):23, https://doi.org/10.1167/tvst.11.8.23

Purpose: The objective of this study was to utilize therapeutic ultrasound in enhancing delivery of topical macromolecules into the cornea.

Methods: Rabbit corneas were dissected and placed in a diffusion cell with a small ultra-red fluorescent protein (smURFP; molecular weight of 32,000 Da) as a macromolecule solution. The corneas were treated with continuous ultrasound application at frequencies of 400 or 600 kHz and intensities of 0.8 to 1.0 W/cm^2 for 5 minutes, or sham-treated. Fluorescence imaging of the cornea sections was used to observe the delivery of macromolecules into individual epithelial cells. Spectrophotometric analysis at smURFP maximal absorbance of 640 nm was done to determine the presence of macromolecules in the receiver compartment. Safety of ultrasound application was studied through histology analysis.

Results: Ultrasound-treated corneas showed smURFP delivery into epithelial cells by fluorescence in the cytoplasm, whereas sham-treated corneas lacked any appreciable fluorescence in the individual cells. The sham group showed 0% of subcellular penetration, whereas the 400 kHz ultrasound-treated group and 600 kHz ultrasound-treated group showed 31% and 57% of subcellular penetration, respectively. Spectrophotometry measurements indicated negligible presence of smURFP macromolecules in the receiver compartment solution in both the sham and ultrasound treatment groups, and these macromolecules did not cross the entire depth of the cornea. Histological studies showed no significant corneal damage due to ultrasound application.

Conclusions: Therapeutic ultrasound application was shown to increase the delivery of smURFP macromolecules into the cornea.

Translational Relevance: Our study offers a clinical potential for a minimally invasive macromolecular treatment of corneal diseases.

Introduction

Ocular drugs are administered by systemic, topical, subconjunctival, intravitreal, and intrascleral delivery.[1–4] Some of these methods are invasive as they may require a needle to penetrate the eye tissue or may require long-term regimen treatments,[1,5] increasing the likelihood of patient non-compliance and leading to lower treatment success rates.[6] The primary method of ocular drug delivery is topical administration, with the cornea being the preferred route despite its small surface area and low permeability.[7–9] Eye drops are noninvasive, easily administered to the cornea, and accessible to a broad patient population.[1,5,10] However, topical eye drops suffer from limited small molecule diffusion across the cornea, resulting in a low bioavailability of approximately 1% to 7% foA2Ar most US Food and Drug Administration (FDA)-approved eye drugs.[4] The bioavailability of macromolecules, including antibodies and proteins, is significantly lower (<1%).[7,10] Topical ocular medications are

usually wasted away by normal tear volume, blinking, and induced lacrimation factors.[10] Ocular delivery is a significant challenge due to multiple eye barriers.[1,5,10] These barriers in the path to successful drug delivery are classified as static or dynamic.[11,12] Static barriers include the corneal epithelium, stroma, endothelium, and blood-aqueous barrier. Dynamic barriers include tear dilution, the conjunctival barrier, and the retinal-blood barrier. The unique structural differences of tissues in the cornea, conjunctiva, retina, and sclera block penetration by toxins, small molecules, viruses, infectious microorganisms, and macromolecules.[13,14] The clinical need is to minimize the time of barrier recovery while maximizing the bioavailability of the administered drug.[15,16] For example, peptide drugs, such as cyclosporine, growth factors, interferons, and interleukins demonstrated treatment of uveitis, corneal wound healing, corneal herpes simplex infections, and modification of ocular immune response. However, most peptide drugs are impermeable when applied topically to the eye due to their high molecular weight.[17] A practical and noninvasive macromolecule delivery method is needed to treat various anterior segment ocular diseases.[4]

In clinical studies, ultrasound-enhanced transcorneal drug delivery treated the eye against anterior segment diseases and corneal inflammation.[18–20] Therapeutic ultrasound offers a promising solution to enhancing ocular delivery with tunable frequencies specific for each tissue, minimal application time, noninvasive delivery, and the ability to combine with a second treatment.[21,22] Our previous in vitro study showed that 5 minutes of ultrasound application of 400 kHz and 600 kHz (at intensities of 0.8 and 1.0 W/cm^2) enhanced the delivery of a small anti-inflammatory molecule (dexamethasone, molecular weight [MW] of 392 Da) into the rabbit cornea.[23] A follow-up in vivo study showed 400 and 600 kHz ultrasound applications at an intensity of 0.8 W/cm^2 resulted in a 2.8- and 2.4-fold increase, respectively, in the delivery of dexamethasone into the aqueous humor.[24] An in vitro study conducted by Lamy et al. in 2013, showed that 880 kHz ultrasound treatment at an intensity of 1.0 W/cm^2 increased the penetration of topically applied riboflavin (MW = 376 Da) into the corneal stroma, regardless of the presence of an intact epithelial barrier.[22] Dexamethasone and riboflavin are approximately 82- and 85-fold smaller than the macromolecule small ultra-red fluorescent protein (smURFP; MW = 32,000 Da) used in this study. The size difference corresponds to a real-life example with an 80-fold change in diameter (D) with a small marble (D = 0.38 inches) for small molecules relative to a large yoga ball (D = 30 inches) for smURFP.

Fluorescence imaging is a helpful noninvasive tool for studying ocular drug delivery. In a previous study by Normand et al. in 2020, whole-eye experiments assessed corneal permeability for different fluorescent small molecules.[25] Another fluorescent imaging study determined corneal permeability levels for small-molecule compounds compared to macromolecules and nanoparticles.[26] Fluorescence imaging of eye autofluorescence and fluorescein angiography is commonly used in clinics and optometrist offices.[27]

A novel far-red fluorescent protein was evolved from the allophycocyanin α-subunit of the phycobilisome and named the smURFP.[28] Far-red fluorescence allows for deeper tissue imaging, and smURFP does not require oxygen or generate hydrogen peroxide upon chromophore formation.[29] The smURFP allows for exogenous, site-specific sortase labeling of membrane proteins to avoid membrane protein misfolding.[30] Herbert and co-workers encapsulated smURFP into viral nanoparticles to noninvasively fluorescently image location, biodistribution, and clearance in living mice.[31] We have previously used smURFP to generate fluorescent protein nanoparticles to image lung cancer xenografts noninvasively, where smURFP fluorescence survived the acidic stomach in living mice.[32] In this study, smURFP was used as the macromolecule to allow for noninvasive corneal imaging and substitute for macromolecule protein drugs.

Materials and Methods

Drug Model

The smURFP was the macromolecule used in our experiments and purified as described in Rodriguez et al. in 2016.[28] Briefly, pBAD smURFP – ribosomal binding site (RBS) – *Synechocystis* heme oxygenase-1 (HO-1) plasmid DNA (#80341; Addgene, Watertown, MA) was transformed in TOP10 *E. coli* (C404010; Thermo Fisher, Waltham, MA) and grown at 37°C in LB supplemented with 50 µg/mL ampicillin (A0166; Millipore Sigma, Burlington, MA) and 0.2% (w/v) arabinose (100706; MP Biomedicals, Irvine, CA) in the dark. Cells were pelleted at 4°C, lysed with B-PER (78243; Thermo Fisher) with DNase I (EN0521; Thermo Fisher) at room temperature, insoluble material was pelleted at 4°C, and the supernatant was saved for protein purification. The supernatant was added to Ni-NTA resin (786940; G-Biosciences, St. Louis, MO), allowed to bind at room temperature by gravity, washed with 50 mM Tris, 300 mM NaCl, and 10 mM imidazole (pH = 7.5), eluted with 50 mM

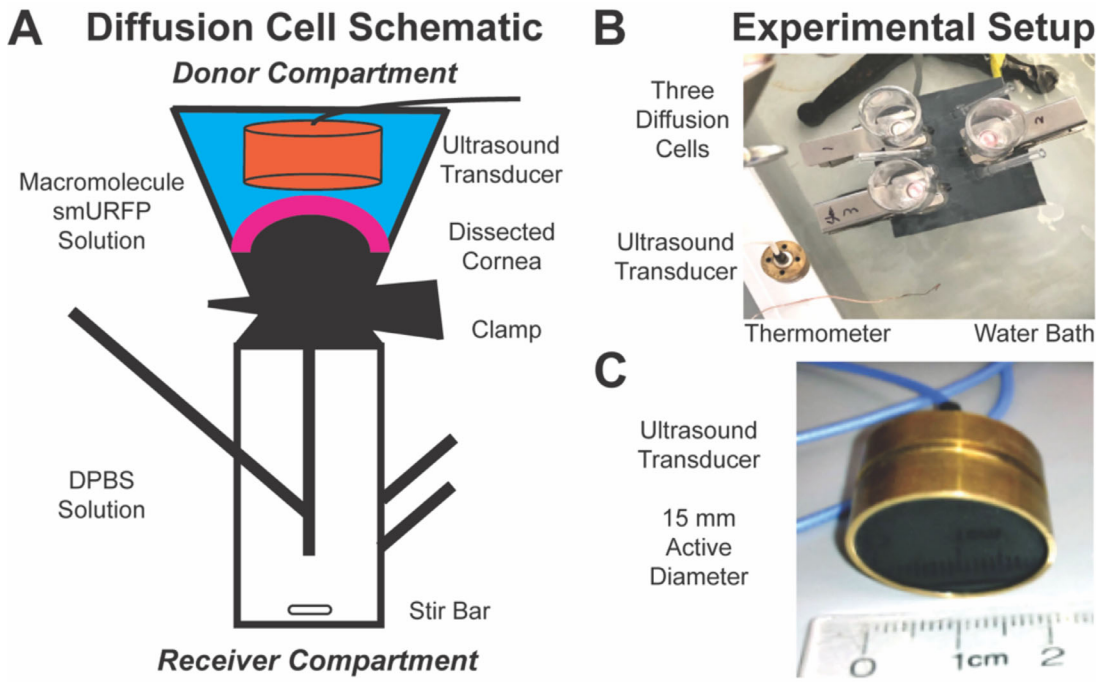

Figure 1. Experimental configuration. (**A**) Diffusion cell schematic. Macromolecule, small ultra-red fluorescent protein (smURFP) is added to the donor compartment (*top*), and Dulbecco's phosphate-buffered saline (DPBS) is added to the receiver compartment (*bottom*). The dissected cornea forms a barrier between the donor and receiver compartments. The transducer is placed in the donor compartment for ultrasound application. Ultrasound is applied to allow macromolecule entry into the corneal epithelium and individual epithelial cells. (**B**) Experimental setup. Three diffusion cells were placed inside a water bath at 34°C with a thermometer also inside the water bath to verify the temperature. The ultrasound transducer (*bottom-left corner*) is shown after it was removed from the donor compartment following the application of ultrasound pulse. (**C**) An example of a custom-designed, circular unfocused 400 kHz ultrasound transducer used in the experiments. The applied ultrasound transducers work at frequencies of 400 or 600 kHz with a 15 mm active diameter.

Tris, 300 mM NaCl, and 200 mM imidazole (pH = 8), and immediately buffer exchanged with PD-10 Desalting Columns (17-0851-01; GE Healthcare, Boston, MA) into phosphate-buffered saline (PBS; pH = 7.4; 10010023; Thermo Fisher). Protein concentration was determined by absorbance at 642 nm using the extinction coefficient of 180,000 M^{-1} cm^{-1} at 642 nm and was stored at 4°C to avoid microbial growth. Concentration was <200 µM smURFP to prevent aggregation and protein precipitation. Sterile filtered smURFP in PBS is stable at room temperature for months without protein precipitation and fluorescence loss.

Animal Model

Healthy adult, New Zealand white rabbit eyes were purchased from Pel-Freez Biologicals (Rogers, AR). In ophthalmic research, rabbit eyes are the most used model for human ocular physiology.[16,33–35] The rabbit eye diameter is 6.5 mm smaller than the human eye. Rabbit cornea is 0.25 mm thinner than the human cornea, whereas the rabbit corneal epithelium is 30 to 40 µm in thickness[36] and thinner than the human epithelium of 50 to 60 µm.[37] The rabbit eyes were harvested immediately after euthanization, stored in Dulbecco's Modified Eagle Medium (DMEM), and shipped overnight on ice. Before use, the rabbit eyes were visually examined to remove the eyes with corneal damage. The eyes were dissected, and the corneas were stored in Dulbecco's phosphate-buffered saline (DPBS; D4031; Millipore Sigma, Burlington, MA) at room temperature for <10 minutes before therapeutic ultrasound experiments.

Experimental Model

Jacketed Franz diffusion cells (PermeGear, Hellertown, PA) were used in the experiments. The orifice diameter is 9 mm, and the volumes of the donor and receiver compartments are 25 and 5 mL, respectively (Fig. 1A). The receiver compartment was filled with 5 mL of DPBS with a magnetic stir bar. The dissected rabbit cornea was clamped with the epithelial layer facing the donor compartment. The donor compartment was filled with 20 mL of 7 µM smURFP in

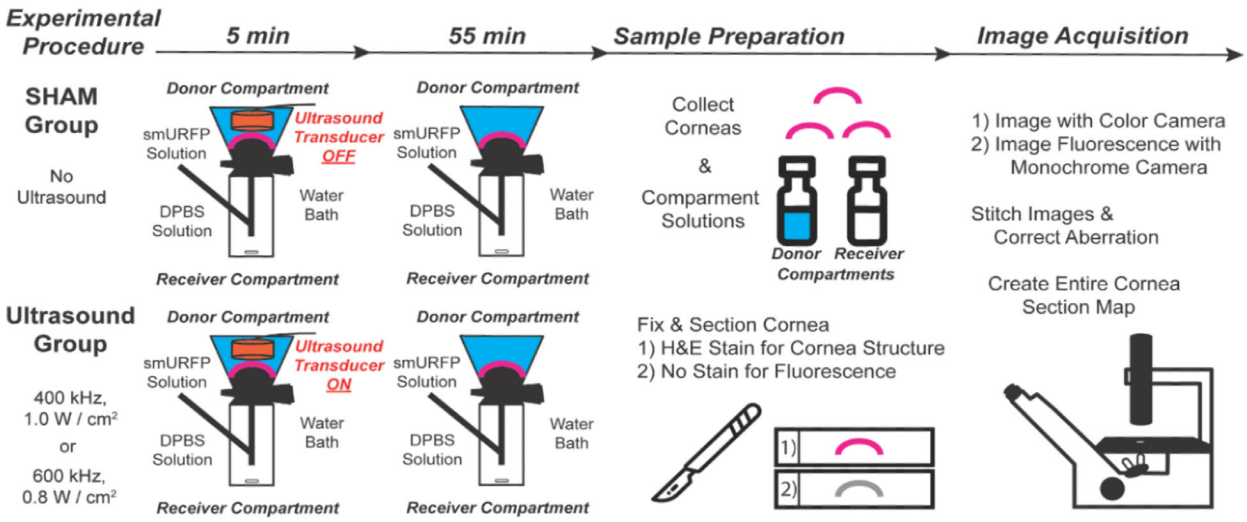

Figure 2. The schematic outlines the experimental procedure and analysis timeline. Dissected corneas are placed in diffusion cells equilibrated in the water bath. The ultrasound transducers are placed above the cornea in a 7 µM smURFP solution. The sham group receives no ultrasound (*top*), and the ultrasound group receives 400 or 600 kHz ultrasound with an intensity of 1.0 or 0.8 W/cm^2, respectively, for 5 minutes. The ultrasound transducers are then removed, and the dissected cornea is allowed to incubate in the diffusion cell for 55 minutes, for a total time of 60 minutes. The dissected corneas are collected for histology processing, and the receiver compartment solution is collected and analyzed for spectrophotometry. Corneas are fixed and sectioned. H&E staining of the cornea sections is performed, and the sections are then imaged with a color camera for structure and damage analysis. Fluorescence imaging is performed on unstained cornea sections to confirm macromolecule smURFP entry into the corneal epithelium, and individual epithelial cells.

PBS (pH = 7.4). Three diffusion cells were placed in the immersion circulator water bath at 34°C and stirred at 380 rpm (Figs. 1A, 1B). Unfocused, custom-designed circular transducers (Sonic Concepts, Bothell, WA) with an active diameter of 15 mm were used for therapeutic ultrasound (Fig. 1C). The entire cornea was exposed to an ultrasound field applied continuously. For optimal energy delivery, the transducer was placed at the near-field to far-field distance from the cornea (d_{ff}) at 1.50 and 2.25 cm for frequencies of 400 kHz (at an intensity of 1.0 W/cm^2) and 600 kHz (at an intensity of 0.8 W/cm^2), respectively.[23] The ultrasound intensity at different input settings was measured using a reflective radiation force balance with an ultrasound power meter (Ohmic Instruments, St. Charles, MO). The driving unit consisted of a function generator (33250; Agilent, Santa Clara, CA) and a power amplifier (150A100B; Amplifier Research, Souderton, PA) connected to the ultrasound transducer by an electrical power meter (Sonic Concepts, Bothell, WA).

A schematic of the timeline of the experimental procedure is shown in Figure 2. In a previous modeling study, 5.5 minutes of ultrasound treatment time was observed to be the length of time for the human eye model to reach the desired cumulative drug concentration.[38] Further, a previously published in vitro study which utilized ultrasound parameters similar to our current parameters showed that 5 minutes of ultrasound application enhanced the delivery of small molecules through the cornea without any significant corneal damage.[23] Therefore, we have selected 5 minutes of treatment time in the current study. We applied 5 minutes of sham treatment (control; ultrasound transducer was turned off) or 5 minutes of ultrasound application. After the experiment, the ultrasound transducer was removed, and the smURFP treated rabbit cornea was incubated for another 55 minutes in the water bath at 34°C. The lag time for the cornea is the minimum time required for a drug to pass through the cornea.[39] The cornea lag time reported for small molecules, such as timolol (MW = 316 Da) and fluorescein (MW = 332 Da), were measured to be 12.0 to 13.0 minutes and 8.5 to 9.0 minutes, respectively.[17,39,40] Macromolecules such as bovine serum albumin (MW = 66,000 Da) and myoglobin (MW = 16,000 Da) have 14.3 hours and 8.20 hours diffusion rate through the ex vivo human cornea, respectively.[41] A study using anti-TNF-α antibody fragment in fresh isolated rabbit cornea showed that ESBA105 (MW = 26,000 Da) penetrated the cornea with 2 hours lag phase, whereas a follow up whole rabbit eyes study showed diffusion of FITC-ESBA105 in the anterior chamber after a lag time of 2 to 3 hours.[42] Based on these previous results, we have decided to test our drug mimicking compound smURFP (MW = 32,000 Da) using a 60 minute experimental time to facilitate

smURFP delivery into deeper layers of the cornea when enhanced with therapeutic ultrasound and to stay consistent with our previously published results that used the same experimental time.[23] After 60 minutes following the start of the experiment, the corneas were collected and separately placed in a glass container with 10% neutral buffered formalin (Fisher Scientific, Waltham, MA). The fixed corneas were then sent for histology preparation (Histoserv Inc., Germantown, MD). Corneal sections were left unstained for monochrome fluorescence imaging (Histoserv Inc.) or stained using hematoxylin and eosin (H&E) staining procedures for color imaging.

Microscopic Imaging

Fluorescence microscopy was performed on unstained corneal sections from 31 experiments and imaged at 23°C using an inverted Zeiss Axio Observer microscope equipped with a monochrome Axiocam503m CCD camera, using a 20 X/0.8 NA air objective (Plan-Apochromat M27; Zeiss, Jena, Germany). For imaging smURFP fluorescence, the excitation/emission was set at 630(13)/709(50) nm and an exposure time was 1.5 seconds (100% LED output). For brightfield images, the transmitted light LED was set at 3.3 V, using an exposure time of 1 second. All images were acquired at 1920 × 1452 pixels with a spatial x-y resolution of 0.2269 micrometer/pixel. The data sets were for sham or no ultrasound (n = 11 in total, and n = 6 and n = 5 for 400 and 600 kHz ultrasound group, respectively), 400 kHz ultrasound (n = 13), and 600 kHz ultrasound (n = 7). The smURFP fluorescence was imaged with excitation and emission of 630(13) and 709(50) nm, respectively, with an exposure time of 1.5 seconds with LED irradiance of 31.54 mW/cm^2. Color images were taken of H&E stained corneal sections and imaged at 23°C using an inverted Thermo Fisher EVOS FL Auto 2 microscope with a color 3.2 MP CMOS camera, using a 4 X/0.13 NA air objective (AMEP4980; Thermo Fisher). The entire H&E stained sections were imaged using transmitted white light, individual images were corrected for objective spherical aberrations, and pictures were stitched together to form a tiled image of the entire corneal section. The raw image files were manipulated, corrected, and quantified in open-source NIH ImageJ.[43] A single 1 µm section was imaged for each of the 31 corneal experiments and accounted for approximately 0.25% of the total corneal area. The scale bars are different in color and fluorescent images because the color and monochrome CCD cameras have different resolutions, and the objectives have different numerical aperture values.

Image Processing

The raw image files of cornea samples (gray LUT, 16-bit) were loaded into ImageJ 1.52s (64- bit) and flat-field background correction was performed with an image of the background signal acquired under identical conditions. Sample and background images were selected with ImageJ tool "Image Calculator Plus" (ImageJ Menu > Process > Calculator Plus) and selecting the option "divide." This step removed variations of the signal in microscopy images due to uneven illumination profile of the light source as well as the noise of the detector. For fluorescent images, the z-stacks were combined using maximum intensity projection option (ImageJ Menu > Image > Stacks > Z-Project > Max. Intensity) and the composite images were used for further processing. Flat-field corrected images were processed to enhance the brightness and contrast (ImageJ Menu > Image > Adjust > Brightness/Contrast) and applying the changes. The low intensity features were enhanced using the Gamma adjusting tool (ImageJ Menu > Process > Math > Gamma > value set at 0.5-1.1). The contrast was improved using the "enhance local contrast tool" (ImageJ Menu > Process > Enhance Local Contrast > set values: blocksize = 25-50; histogram = 256; and maximum slope = 1.75). The final adjustment enhanced the sharpness of the image and eliminated the excessive blur, which was done using the advanced sharpening tool (ImageJ Menu > Process > Filters > Unsharp Mask > Radius = 20-30 pixels; weight = 0.3 – 0.35).

Structural Changes

Structural changes in the H&E-stained corneal sections were analyzed and imaged using an upright ZeissAxio Imager (Carl Zeiss Inc., Jena, Germany). The 1 µm thick corneal sections were imaged with a 40 X/0.65 NA air objective (A-Plan; Carl Zeiss Inc.) and 10 X/0.25 NA air objective (N-Achroplan; Carl Zeiss Inc.). Histological observations of corneal damages were performed using a modified method described by Nabili et al. in 2014.[24] Briefly, different classes of corneal damage were defined as follows: class 1 (no damage) = the three cornea layers are discernible as epithelium, stroma, and endothelium. Cell nuclei are visible in the epithelium. Class 2 = the three corneal layers are visualized. Epithelial layers appear slightly damaged, and the cellular structure is more challenging to observe. The endothelium is intact. Class 3 = only two layers are discernible as epithelium and stroma, with more substantial damage observed in the epithelium. Class 4 = the corneal tissue is damaged, and the

layers are not identifiable. The H&E-stained corneal sections were imaged to identify structural changes to verify therapeutic ultrasound safety in ocular tissues.

Spectrophotometry

The receiver compartment solutions were collected with a glass pipette, and the absorbance was measured using a SpectraMax ID5 (Molecular Devices, San Jose, CA). The receiver compartment absorbance was measured at 640 nm, the wavelength of maximum absorbance of the smURFP fluorophore, to determine the macromolecule concentration in the receiver compartment solution.[44] The unpaired *t*-test assuming unequal variances was used to compare the receiver absorbance distribution of the sham and each ultrasound group. The one-way analysis of variance (ANOVA; single factor) test was used to compare the distribution of all the three groups, followed by Tukey's post hoc test to determine which groups were considered significant. The null hypothesis states there is no difference between the groups, whereas the alternative hypothesis is that the groups are different. Differences were considered statistically significant at $P < 0.05$, which allowed the null hypothesis to be rejected. Absorbance measurements of the receiver compartment were performed for the no ultrasound (sham) group ($n = 11$), the 400 kHz ultrasound group ($n = 13$), and the 600 kHz ultrasound group ($n = 7$). Additional spectrophotometric study of negative control corneas that were kept for 60 minutes in a water bath with DPBS buffer only without smURFP and without ultrasound application was done to observe whether the diffusion of biological compounds from the cornea into the receiver compartment is affecting the measurements of the ultrasound and sham groups.[39]

Results

Microscopic Imaging

Unstained, fixed corneal sections ($n = 31$) were fluorescently imaged to directly image the probe in rabbit tissue without secondary detection, such as immunohistochemistry or immunofluorescence. Experiments confirmed that the fluorescence of smURFP survives ultrasound application and formalin fixation. The sham group ($n = 11$) showed 0%

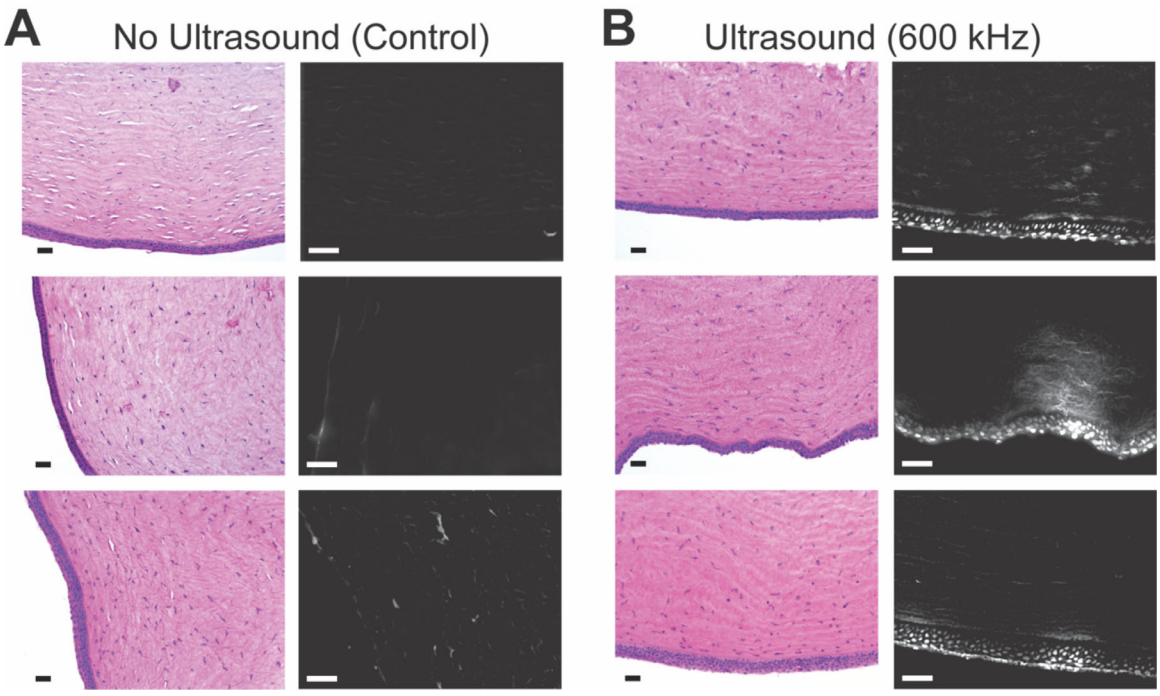

Figure 3. Representative images showing the anterior cornea epithelium. Corneas were incubated with 7 µM smURFP and received (**A**) control (sham treatment) or (**B**) ultrasound (600 kHz with an applied intensity of 0.8 W/cm^2) for 5 minutes. Brightfield, colored images, and fluorescence, monochrome images are shown on the *left* and *right*, respectively. **A** Control (sham) experiments show dim fluorescence. **B** Ultrasound delivers smURFP to the interior of the epithelium and inside individual epithelial cells. Control (sham treatment) images **A** do not show fluorescence inside the epithelium or the cells. The scale bar is 50 µm.

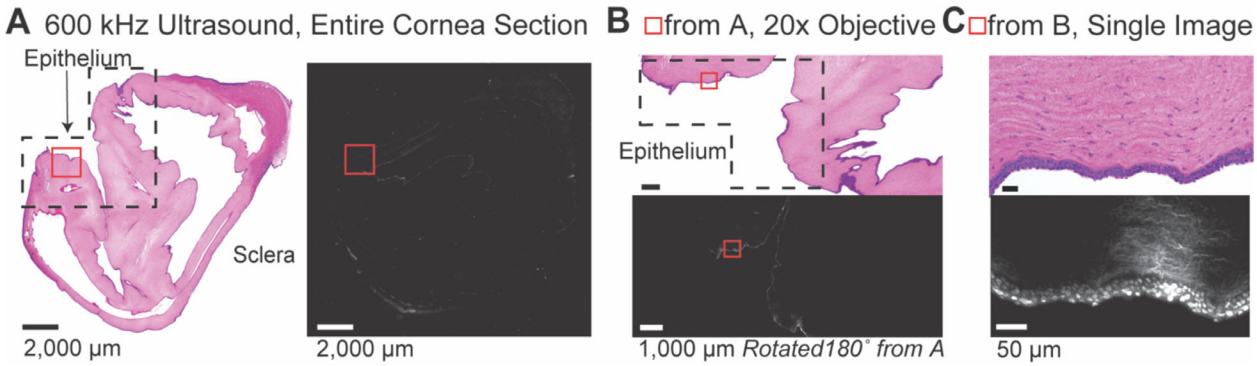

Figure 4. Representative images of an ultrasound-treated cornea. (**A**) Entire cornea section. Tears result from the sectioning of the cornea dome. The outer cornea is exposed to smURFP and shows the greatest fluorescence. (**B**) Twenty times (20 X) objective image of the *red square* in **A** rotated 180 degrees. The epithelium layer shows the fluorescence of the smURFP macromolecule. (**C**) A single image from the *red square* in **B**. Single epithelium cells show uptake of smURFP and deeper fluorescence in the stroma. We have entire cornea images for 31 cornea experiments, and additional examples are shown in Figure 5.

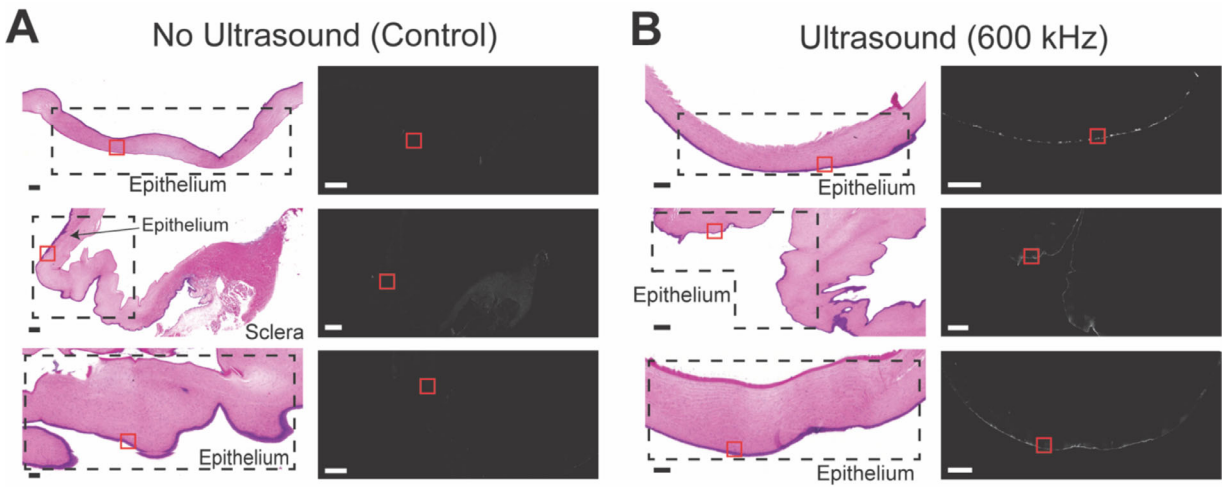

Figure 5. Representative images of whole cornea epithelium. Corneas are incubated with 7 µM smURFP received (**A**) control (sham treatment) or (**B**) ultrasound (600 kHz with applied intensity of 0.8 W/cm^2) for 5 minutes. Brightfield, colored images, and fluorescence, monochrome images are shown on *left* and *right*, respectively. **A** Control (sham treatment) experiments show weak fluorescence on the exterior of the epithelium or the sclera. **B** Ultrasound delivers fluorescent proteins to the interior of the epithelium. The anterior face of the epithelium and the sclera are labeled. The cornea epithelium is enclosed in a *black dashed box*. The *red boxes* show the locations imaged at higher magnification (20 X), shown in Figure 3. The scale bar is 2000 µm.

of subcellular penetration, whereas the 400 kHz ultrasound-treated group ($n = 13$) and the 600 kHz ultrasound-treated group ($n = 7$) showed approximately 31% and 57% of subcellular penetration, respectively. In Figures 3–5, the entire cornea was not imaged, and only a single corneal section of 1 µm thickness was imaged. Untreated corneas displayed nonspecific fluorescence on the outer surface of the epithelium exposed to the donor compartment smURFP solution (see Fig. 3A). Figure 3B shows subcellular delivery of the macromolecule smURFP in the epithelium and stroma of 600 ultrasound-treated corneas compared to the sham group. We have obtained whole corneal section images ($n = 31$) from our experiments with representative examples shown in Figures 4 and 5. Thousands of 20 X objective images were stitched to create a map of each corneal section and allowed imaging of corneal structure damage and smURFP delivery into individual cells. A representative whole cornea section (approximately 1.4 cm) treated with an ultrasound application of 600 kHz at 0.8 W/cm^2 magnified to a single image 425 µm in length (approximately 3,300 X magnification) is shown in Figure 4. Overall, 40 percent of

Table. Classification of Corneal Structural Changes in the Sham and Ultrasound Groups

Group	Class 1	Class 2	Class 3	Class 4	Total
Sham no ultrasound	10	1	0	0	11
Ultrasound 400 kHz and 1.0 W/cm^2	5	3	4	1	13
Ultrasound 600 kHz and 0.8 W/cm^2	4	3	0	0	7

Class 1 (no damage) = The three cornea layers are discernible as epithelium, stroma, and endothelium. Cell nuclei in the epithelium are visible. **Class 2** = The three corneal layers are visualized. Epithelial layers appear slightly damaged, and cellular structure is more challenging to observe. The endothelium is intact. **Class 3** = Only two layers are discernible as epithelium and stroma, with more substantial damage observed in the epithelium. **Class 4** = Corneal tissue is damaged, and layers are not identifiable.

the corneas ($n = 20$) treated with either 400 kHz or 600 kHz ultrasound showed smURFP delivery into individual cells in the epithelium. In comparison, no delivery (0%) was observed in the sham-treated group ($n = 11$).

Structural Changes

Histological observations of corneal damages of the sham ($n = 11$), the 400 kHz ultrasound-treated ($n = 13$), and the 600 kHz ultrasound-treated ($n = 7$) groups are shown in the Table. Histology imaging showed minor changes in the surface of the epithelium in the sham and 600 kHz ultrasound-treated at 0.8 W/cm^2 groups. In contrast, the application of 400 kHz at 1.0 W/cm^2 ultrasound produced more damage when compared to the sham group (see the Table). Histological comparisons between sham and 600 kHz ultrasound-treated corneas are shown in Figure 3.

Spectrophotometry

Absorbance values were 0.08 ± 0.021 ($n = 11$), 0.09 ± 0.060 ($n = 13$), and 0.08 ± 0.002 ($n = 7$; mean ± SD) in the sham, 400 kHz, and 600 kHz groups, respectively. Spectrophotometric analysis of the receiver compartment solution at the smURFP maximal absorbance of 640 nm indicated that there was no statistical difference ($P > 0.05$, unpaired t-test, and 1-way ANOVA) among the three groups (Fig. 6). The absorbance measurements indicated negligible smURFP macromolecules in the receiver compartment in both the sham and ultrasound treatment groups, and smURFP does not cross the entire depth of the cornea in these experiments. The values for negative control absorbance of the sham, the 400 kHz, and the 600 kHz groups (mean ± SD) were: 0.09 ± 0.005 ($n = 3$), 0.11 ± 0.020 ($n = 3$), and 0.08 ± 0.001 ($n = 3$), respectively. No significant difference was detected among the groups which indicated that biological diffusion would not affect our ultrasound and sham spectrophotometric data.[39]

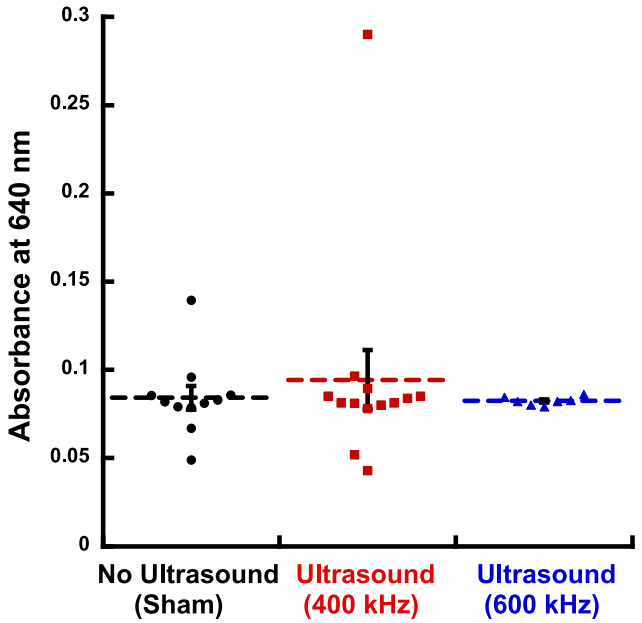

Figure 6. Absorbance of the receiver compartment solution determined at smURFP absorbance maximum of 640 nm. Sham group ($n = 11$), 400 kHz ultrasound group ($n = 13$), and 600 kHz ultrasound group ($n = 7$). The *dashed, horizontal lines* are the means and the error bars are the standard error of the mean (SEM). Absorbance measurements indicate no statistical difference among the sham and both ultrasound groups.

Discussion

Previous studies[23,24] showed that therapeutic ultrasound can be applied safely to the eye and may offer a noninvasive method for corneal drug delivery. Our smURFP macromolecules allowed for ultrasound optimization and visualization of macromolecule delivery. Ultrasound application and formalin fixation did not diminish smURFP fluorescence in the tissues, and smURFP is a useful macromolecule probe to visualize ultrasound-enhanced delivery into individual corneal cells. Many far-red small molecule fluorophores, including AlexaFluor647 and Cy5,

and near-infrared bacterial phytochrome fluorescent proteins do not survive fixation or protease treatment for use in tissue clearing and expansion microscopy.[45] Our experiments illustrate the power of fluorescence visualization to show ultrasound delivery of macromolecules into the epithelium, anterior stroma, and keratocytes (see Figs. 3–5). Our results suggest that smURFP may be a practical far-red and near-infrared alternative to AlexaFluor647, Cy5, and infrared fluorescent proteins (IFPs and iRFPs) in fixed tissue for expansion microscopy. The smURFP fluorescence was stable in formalin-fixed, unstained corneal sections for months. In addition, smURFP is a self-labeling protein that allows for the chromophore to be modified to covalently attach to proteins, antibodies, and biomolecules to directly image the location of ultrasound-delivered macromolecules.[46]

Ultrasound-treated corneas (600 kHz) showed macromolecule fluorescence in the individual epithelium and stromal cells in 57% of the imaged corneal sections. None of the sham-treated corneal sections showed fluorescence in individual cells. Although 40% penetration of all ultrasound groups does not seem high, we only imaged a single corneal section that was 1 µm thick from each sample. Because the rabbit cornea is 407 ± 20 µm in thickness,[47] we only imaged approximately 0.25% of the cornea. Imaging all corneal sections would increase the likelihood of finding individual cells with macromolecules for a more statistically significant comparison.

Absorbance measurements of the receiver compartment indicated no statistical differences between the sham and both ultrasound groups. Given the negligible presence of smURFP molecules in the receiver compartment of our ultrasound-treated eyes, our experiments showed that the corneal barrier was not ruptured between the donor and receiver compartments due to the application of ultrasound. Because there is no difference between the sham and ultrasound groups, the absorbance measurements indicated that ultrasound application does not destroy or cause a sizable transient rupture to the corneal barrier to nonspecifically allow the passage of macromolecules across the barrier to the receiver compartment in the diffusion cell setup. Maintaining the corneal barrier is clinically essential to avoid infections and loss of sight after treatment.

Histological studies indicated only minor changes in the surface of the epithelium in the sham groups and 600 kHz ultrasound group at an intensity of 0.8 W/cm^2. However, the 400 kHz ultrasound group at an intensity of 1.0 W/cm^2 showed more damage, and the damage was predominantly classified as class 3. Some of the observed corneal damage, especially in the endothelium, was probably due to histological processing artifacts.[48] Although ultrasound application at 400 kHz is at a lower frequency, the intensity is slightly higher at 1.0 W/cm^2 for 400 kHz relative to 0.8 W/cm^2 for 600 kHz. Generally, cavitation effects increase at lower ultrasound frequencies and lead to more damage.[49] Higher intensity also increases undesirable biological damage.[49] The published literature confirms our observations of more corneal damage seen at lower ultrasound frequencies and higher intensities.[24] Delivery of macromolecules in the cornea appears to be optimal at ultrasound parameters of 0.8 W/cm^2 and 600 kHz to allow for delivery of macromolecules into individual cells without damaging the tissue. Additional future studies of the structural effects of ultrasound on diseased eyes are needed as a follow up to test our approach in clinically relevant situations. Future experiments should incorporate in vivo studies in a rabbit model before subsequent clinical trials.

Cell permeability to small molecules is enhanced by ultrasound cavitation, where bubbles in the liquid form and subsequently collapse.[50,51] The most critical mechanism in corneal transport is the diffusion of compounds in the epithelium, namely, the porosity.[38] In addition to cavitation, ultrasound-induced thermal changes may play a role in enhancing corneal permeability, although they raise a safety concern.[34] Our previous ocular thermal safety modeling studies that utilized similar ultrasound parameters demonstrated maximal temperature increases in the cornea of 1.0°C at 400 kHz and 1.5°C at 600 kHz with intensities of 1.0 and 0.8 W/cm^2, respectively.[52] The change of 1.0°C and 1.5°C is minimal and less than exposure to sun on a summer day.[53] Within aforementioned thermal range for the eye, therapeutic ultrasound may offer a less invasive solution for delivery of macromolecules into the cornea.

Challenges that need to be addressed in ocular delivery of macromolecules include reducing treatment frequency when administered by a healthcare professional, increasing drug targeting to the diseased site to increase effectiveness and safety, and increasing the bioavailability of extraocular delivery methods.[4,54] Ocular injections are associated with vision improvement; however, ophthalmologists have recognized the burden of poor patient compliance and lack of treatment tolerance.[55–59] An ultrasound approach for the delivery of macromolecular drugs may lead to improved patient outcomes in terms of higher treatment compliance and avoidance of side effects associated with more invasive treatment options.[6] Ultrasound has several advantages, including noninvasive application, short exposure times, flexibility in

adjusting delivery parameters, and the ability to be applied with standard ophthalmic drugs, and easily combined with other drug delivery methods.[23,33,54] As a current treatment example, the anti-fungal drugs are typically administered every hour immediately after corneal debridement or for the first several days of therapy.[60] The eye drop application is then continued hourly during waking hours for 3 days (at least 9 times/day is recommended) depending on clinical response. Our proposed ultrasound application may allow for faster and less invasive treatment. Further, our approach is the first to utilize smURFP molecules in ocular applications. Although we have published on application of ultrasound in enhancing corneal drug delivery,[23,24,35,38] our previous work was only focused on small molecules, and this is our first study with macromolecules.

Antibodies, CRISPR/Cas9 + gRNA, therapeutic proteins, mRNA, DNA, and other macromolecules can treat human diseases and blindness. In ocular applications, macromolecules require appropriate administration routes and vectors to establish safety, efficiency, and specificity in delivery.[61] Whereas outside of the scope of the current study, it would be important to test the effect of ultrasound on macromolecules and their therapeutic efficacy for each of the macromolecules that are of potential interest in ocular applications. A recent study showed successful hair growth in alopecia animals using the CRISPR/Cas9 + gRNA system delivered by nano-carrier technology to enhance the efficiency and specific targeting when agitated by ultrasound activation.[62] This strategy applies to treating corneal diseases using nano-carriers or fluorescent protein nanoparticles[32] to deliver CRISPR/Cas9 + gRNA. A previous study showed that local injection of CRISPR/Cas9 + gRNA in the rat eyes treated non-hereditary diseases, such as wet age-related macular degeneration (AMD), and is in preclinical trials.[63] CRISPR/Cas9 + gRNA should be deliverable by ultrasound to treat ocular diseases, and smURFP is of similar molecular weight to allow fluorescence visualization of macromolecule delivery in research applications.

Our ultrasound approach can be a minimally invasive option for treating various corneal disorders, including infections, keratoconus, or corneal genetic disorders.[23,64–66] For example, keratoconus is a noninflammatory and asymmetric corneal ectasia which results in progressive bulging out and thinning of the cornea that severely impairs visual acuity.[67,68] Current keratoconus treatment is depending on the severity and progression of the disease, starting from glasses and contact lens to corneal surgeries.[67–69] Surgical intervention, such as corneal collagen cross linking, intracorneal ring segment, and corneal grafting, are promising approaches for patients with keratoconus, yet they have post-surgery adverse effects such as infections, pain, and/or inflammation.[68,70,71] Overall, if successful, our proposed technology may lead to a change in the standard of care and may lower the post-surgery complications and increase patient compliance.

In this study, we used smURFP as a mimic for macromolecule drugs that are used for ocular diseases. Most of the FDA approved topical ocular drugs for anterior segment are small molecules, including Tyrvaya, Restasis, Xiidra, and Eysuvis.[72] Most of the FDA approved macromolecular ocular drugs are invasively delivered due to their low ocular targeting and bioavailability.[4] For example, ocular macromolecule bevacizumab (MW = 149,196 Da) applied topically on intact cornea has limited capacity to penetrate even into the very superficial layer of the cornea and need to be delivered via intraocular injections.[73] In comparison, smURFP (MW = 32,000 Da) was showing 31% and 57% subcellular penetration into the cornea in the 400 kHz and 600 kHz ultrasound groups. Although outside of the scope of the current study, it would be important to test the effectiveness of ultrasound in enhancing delivery of a range of molecular weights used in the treatment of anterior segment eye diseases.

Acknowledgments

The authors thank Papa Lab (GW, Department of BME) for the guidance during the absorbance measurements. We also thank Mary Ann Stepp for her help with the conception of this project.

Funded by the George Washington University (GW) Cross-Disciplinary Research Fund awarded to Zderic, Rodriguez, and Stepp and the GW Cancer Center and Katzen Research Cancer Research Pilot Award awarded to Rodriguez.

Conflict of Interest Statement: The authors certify that they have no affiliations with or involvement in any organization or entity with any financial interest or non-financial interest in the subject matter or materials discussed in this manuscript.

Disclosure: **H.H. Almogbil**, None; **F. Montecinos-Franjolz**, None; **C. Daszynski**, None; **W.J. Conlon**, None; **J.S. Hachey**, None; **G. Corazza**, None; **E.A. Rodriguez**, None; **V. Zderic**, None

References

1. Short BG. Safety evaluation of ocular drug delivery formulations: techniques and practical considerations. *Toxicol Pathol*. 2008;36:49–62.
2. Kompella UB, Kadam RS, Lee VHL. Recent advances in ophthalmic drug delivery. *Ther Deliv*. 2011;1:435–456.
3. Molokhia SA, Thomas SC, Garff KJ, Mandell KJ, Wirostko BM. Anterior eye segment drug delivery systems: Current treatments and future challenges. *J Ocul Pharmacol Ther*. 2013;29:92–105.
4. Kim YC, Chiang B, Wu X, Prausnitz MR. Ocular delivery of macromolecules. *J Control Release*. 2014:190;172–181.
5. Mandal A, Pal D, Agrahari V, Trinh HM, Joseph M, Mitra AK. Ocular delivery of proteins and peptides: Challenges and novel formulation approaches. *Adv Drug Deliv Rev*. 2018;128:67–95.
6. Polat O, Inan S, Ozcan S, et al. Factors affecting compliance to intravitreal anti-vascular endothelial growth factor therapy in patients with age-related macular degeneration. *Turk J Ophthal*. 2017;47:205–210.
7. Achouri D, Alhanout K, Piccerelle P, Andrieu V. Recent advances in ocular drug delivery. *Drug Dev Ind Pharm*. 2013;39:1599–1617.
8. Ahmed I, Patton TF. Disposition of timolol and inulin in the rabbit eye following corneal versus non-corneal absorption. *Int Journal Pharm*. 1987;38:9–21.
9. Davies NM. Biopharmaceutical considerations in topical ocular drug delivery. *Clin Exp Pharmacol Physiol*. 2000;27:558–562.
10. Gaudana R, Ananthula HK, Parenky A, Mitra AK. Ocular drug delivery. *AAPS J*. 2010;12:348–360.
11. Gote V, Sikder S, Sicotte J, Pal D. Ocular drug delivery: Present innovations and future challenges. *J Pharm Exp Ther*. 2019;370:602–624.
12. Peynshaert K, Devoldere J, De Smedt SC, Remaut K. In vitro and ex vivo models to study drug delivery barriers in the posterior segment of the eye. *Adv Drug Deliv Rev*. 2018;126:44–57.
13. Suri R, Beg S, Kohli K. Target strategies for drug delivery bypassing ocular barriers. *J Drug Deliv Sci Technol*. 2019;55:101389.
14. Agrahari V, Mandal A, Agrahari V, et al. A comprehensive insight on ocular pharmacokinetics. *Drug Deliv Transl Res*. 2016:6;735–754.
15. Irimia T, Ghica MV, Popa L, Anuta V, Arsene AL, Dinu-Pîrvu CE. Strategies for improving ocular drug bioavailability and corneal wound healing with chitosan-based delivery systems. *Polymers*. 2018;10:1221.
16. Almogbil HH, Nasrallah FP, Zderic V. Feasibility of therapeutic ultrasound application in topical scleral delivery of Avastin. *Transl Vis Sci Technol*. 2021;10:2.
17. Sasaki H, Igarashi Y, Nagano T, Yamamura K, Nishida K, Nakamura J. Penetration of β-blockers through ocular membranes in albino rabbits. *J Pharm Pharmacol*. 1995;47:17–21.
18. Cherkasov IS, Marmur RK, Radkovskaia AI, Loskova LM. Phonophoresis of hypotensive agents in the treatment of simple glaucoma. *Opthalmol Zh*. 1974;29:114–118.
19. Filippenko V, Tretiak V. The treatment of eye diseases using the Gamma-G ultrasonic apparatus. *Voen Med Zh*. 1989;8:30–31.
20. Tsok RM. Primenenie fonoforeza pri nekotorykh zabolevaniiakh perednego otrezka glaza. *Oftalmol Zh*. 1979;34:73–76.
21. Huang D, Wang L, Dong Y, Pan X, Li G, Wu C. A novel technology using transscleral ultrasound to deliver protein loaded nanoparticles. *Eur J Pharm Biopharm*. 2014;88:104–115.
22. Lamy R, Chan E, Zhang H, et al. Ultrasound-enhanced penetration of topical riboflavin into the corneal stroma. *Invest Ophthalmol Vis Sci*. 2013;54:5908–5912.
23. Nabili M, Patel H, Mahesh SP, Liu J, Geist C, Zderic V. Ultrasound-enhanced delivery of antibiotics and anti-inflammatory drugs into the eye. *Ultrasound Med Biol*. 2013;39:638–646.
24. Nabili M, Shenoy A, Chawla S, et al. Ultrasound-enhanced ocular delivery of dexamethasone sodium phosphate: An in vivo study. *J Ther Ultrasound*. 2014;2:6.
25. Normand G, Maker M, Penraat J, et al. Non-invasive molecular tracking method that measures ocular drug distribution in non-human primates. *Commun Biol*. 2020;3:1–11.
26. Mun EA, Morrison PWJ, Williams AC, Khutoryanskiy VV. On the barrier properties of the cornea: A microscopy study of the penetration of fluorescently labeled nanoparticles, polymers, and sodium fluorescein. *Mol Pharm*. 2014;11:3556–3564.
27. Schwartz SD, Regillo CD, Lam BL, et al. Human embryonic stem cell-derived retinal pigment epithelium in patients with age-related macular degeneration and Stargardt's macular dystrophy: Follow-up of two open-label phase 1/2 studies. *Lancet*. 2015;385:509–516.
28. Rodriguez EA, Tran GN, Gross LA, et al. A far-red fluorescent protein evolved from a cyanobac-

terial phycobiliprotein, *Nat Methods*. 2016;13:763–769.
29. Montecinos-Franjola F, Lin JY, Rodriguez EA. Fluorescent proteins for in vivo imaging, where's the biliverdin?, *Biochem Soc Trans*. 2020;48:2657–2667.
30. Deshpande I, Liang J, Hedeen D, et al. Smoothened stimulation by membrane sterols drives Hedgehog pathway activity. *Nature*. 2019;571:284–288.
31. Herbert FC, Brohlin OR, Galbraith T, et al. Supramolecular encapsulation of small-ultrared fluorescent proteins in virus-like nanoparticles for noninvasive in vivo imaging agents. *Bioconjug Chem*. 2020;31:1529–1536.
32. An F, Chen N, Conlon WJ, et al. Small ultrared fluorescent protein nanoparticles as exogenous probes for noninvasive tumor imaging in vivo. *Int J Biol Macromol*. 2020;153:100–106.
33. Cheung ACY, Yu Y, Tay D, Wong HS, Ellis-Behnke R, Chau Y. Ultrasound-enhanced intrascleral delivery of protein. *Int J Pharm*. 2010;401:16–24.
34. Allison C, Cellum B, Karpinecz B, Nasrallah F, Zderic V. Ultrasound-enhanced transcorneal drug delivery for treatment of fungal keratitis. *Cornea*. 2022; 41:894–900.
35. Karpinecz B, Edwards N, Zderic V. Therapeutic ultrasound-enhanced transcorneal PHMB delivery in vitro. *J Ultrasound Med*. 2021;40:2561–2570.
36. Tsonis P. *Animal Models in Eye Research*. 1st ed. New York, NY: Elsevier; 2008.
37. Snell R, Lemp M. *Clinical Anatomy of the Eye*. 2nd ed. England: Blackwell Science, Inc.; 1998.
38. Hariharan P, Nabili M, Guan A, Zderic V, Myers M. Model for porosity changes occurring during ultrasound-enhanced transcorneal drug delivery. *Ultrasound Med Biol*. 2017;43:1223–1236.
39. Zderic V, Vaezy S, Martin RW, Clark JI. Ocular drug delivery using 20-kHz ultrasound. *Ultrasound Med Biol*. 2002;28:823–829.
40. Araie M, Maurice D. The rate of diffusion of fluorophores through the corneal epithelium and stroma. *Exp Eye Res*. 1987;44:73–87.
41. Charalel RA, Engberg K, Noolandi J, Cochran JR, Frank C, Ta CN. Diffusion of Protein Through the Human Cornea. *Ophthalmic Res*. 2012;48(1):50.
42. Ottiger M, Thiel MA, Feige U, Lichtlen P, Urech DM. Efficient Intraocular Penetration of Topical Anti–TNF-α Single-Chain Antibody (ESBA105) to Anterior and Posterior Segment without Penetration Enhancer. *Invest Ophthal Vis Sci*. 2009;50:779–786.
43. Schneider CA, Rasband WS, Eliceiri KW. NIH Image to ImageJ: 25 years of image analysis. *Nat Methods*. 2012;9:671–675.
44. Rodriguez E, Lin J, Tsien R, Ting R, Tran G. Allophycocyanin alpha-subunit evolved labeling proteins (smURFPs). Patent US-2018201655-A1. PubChem, 2016, https://pubchem.ncbi.nlm.nih.gov/patent/US2018201655. Accessed April 29, 2021.
45. Gao R, Asano SM, Boyden ES. Q & A: Expansion microscopy. *BMC Biol*. 2017:15:50.
46. Machado JH, Ting R, Lin JY, Rodriguez EA. A self-labeling protein based on the small ultra-red fluorescent protein, smURFP. *RSC Chem Biol*. 2021;2:1221–1226.
47. Chan T, Payor S, Holden BA. Corneal thickness profiles in rabbits using an ultrasonic pachometer. *Invest Ophthalmog Vis Sci*. 1983;24:16–24.
48. Zderic V, Clark JI, Martin RW, Vaezy S. Ultrasound-enhanced transcorneal drug delivery. *Cornea*. 2004:23:804–811.
49. Miller DL, Smith NB, Bailey MR, Czarnota GJ, Hynynen K, Makin IRS. Overview of therapeutic ultrasound applications and safety considerations. *J Ultrasound Med*. 2012;31:623–634.
50. Lawrie A, Brisken AF, Francis SE, et al. Ultrasound enhances reporter gene expression after transfection of vascular cells in vitro. *Circulation*. 1999;99:2617–2620.
51. Zderic V, Clark JI, Vaezy S. Drug delivery into the eye with the use of ultrasound. *J Ultrasound Med*. 2004;23:1349–1359.
52. Nabili M, Geist C, Zderic V. Thermal safety of ultrasound-enhanced ocular drug delivery: A modeling study. *Med Phys*. 2015;42:5604–5615.
53. Rosenthal F, Phoon C, Bakalian JAE, Taylor HR. The ocular dose of ultraviolet radiation to outdoor workers. *Invest Ophthalmol Vis Sci*. 1988;29:649–656.
54. Aptel F, Lafon C. Therapeutic applications of ultrasound in ophthalmology. *Int J Hyperthermia*. 2012;28:405–418.
55. Mulligan K, Seabury SA, Dugel PU, Blim JF, Goldman DP, Humayun MS. Economic value of anti–vascular endothelial growth factor treatment for patients with wet age-related macular degeneration in the United States. *JAMA Ophthalmol*. 2020;138:40–47.
56. Boyer DS, Hopkins JJ, Sorof J, Ehrlich JS. Anti-vascular endothelial growth factor therapy for diabetic macular edema. *Ther Adv Endocrinol Metab*. 2013;4:151–169.
57. Ghasemi Falavarjani K, Nguyen QD. Adverse events and complications associated with intravit-

real injection of anti-VEGF agents: a review of literature. *Eye* 2013;27:787–794.
58. Shikari H, Silva PS, Sun JK. Complications of intravitreal injections in patients with diabetes. *Semin Ophthalmol*. 2014;29:276–289.
59. Shin SH, Park SP, Kim YK. Factors associated with pain following intravitreal injections. *Korean J Ophthal*. 2018;32:196–203.
60. Wang JY, Wang DQ, Qi XL, Cheng J, Xie LX. Modified ulcer debridement in the treatment of the superficial fungal infection of the cornea. *Int J Ophthalmol*. 2018;11:223–229.
61. Yu W, Wu Z. Ocular delivery of CRISPR/Cas genome editing components for treatment of eye diseases. *Adv Drug Deliv Rev*. 2021;168:181–195.
62. Ryu JY, Won EJ, Lee HAR, et al. Ultrasound-activated particles as CRISPR/Cas9 delivery system for androgenic alopecia therapy. *Biomaterials*. 2020;232:119736.
63. Kim K, Park SW, Kim JH, et al. Genome surgery using Cas9 ribonucleoproteins for the treatment of age-related macular degeneration. *Genome Res*. 2017;27:419–426.
64. Almogbil H, Daszynski C, Rodriguez EA, Singh T, Stepp MA, Zderic V. Therapeutic ultrasound for improving topical delivery of macromolecules. *177th Meeting of the Acoustic Society of America (Abstract), Louisville, KY, 2019*, https://acousticalsociety.org/program-of-177th-meeting/.
65. Mohan RR, Sharma A, Netto MV, Sinha S, Wilson SE. Gene therapy in the cornea. *Prog in Retin Eye Res*. 2005;24:537–559.
66. Mohan RR, Rodier JT, Sharma A. Corneal gene therapy: Basic science and translational perspective. *Ocul Surf*. 2013;11:150–164.
67. Romero-Jiménez M, Santodomingo-Rubido J, Wolffsohn JS. Keratoconus: A review. *Contact Lens Anterior Eye*. 2010;33:157–166.
68. Xue Y, Zhou J, Chen Z, et al. Factors affecting long-term compliance with rigid gas-permeable contact lens wear in patients with keratoconus. *J Clin Med*. 2022;11:1091.
69. Santodomingo-Rubido J, Carracedo G, Suzaki A, Villa-Collar C, Vincent SJ, Wolffsohn JS. Keratoconus: An updated review. *Contact Lens Anterior Eye*. 2022;45(3):101559.
70. Sakellaris D, Balidis M, Gorou O, et al. Intracorneal ring segment implantation in the management of keratoconus: an evidence-based approach. *Ophthalmol Ther*. 2019;8(Suppl 1):5–14.
71. Dhawan S, Rao K, Natrajan S. Complications of corneal collagen cross-linking. *J Ophthalmol*. 2011;2011:1–5.
72. Mukamal R, Starr CE. *Improved dry eye drugs for 2022 and beyond*. American Academy of Ophthalmology (AAO). 2022, https://www.aao.org/eye-health/tips-prevention/new-dry-eye-treatments-ocular-surface-disease.
73. Dastjerdi MH, Sadrai Z, Saban DR, Zhang Q, Dana R. Corneal penetration of topical and subconjunctival bevacizumab. *Invest Ophthalmol Vis Sci*. 2011;52:8718–8723.